

Photoneutron cross sections for ^{55}Mn and ^{59}Co

R. A. Alvarez, B. L. Berman, D. D. Faul, F. H. Lewis, Jr., and P. Meyer

Lawrence Livermore Laboratory, University of California, Livermore, California 94550

(Received 5 February 1979)

Photoneutron cross sections, including $\sigma[(\gamma, n) + (\gamma, pn)]$, $\sigma(\gamma, 2n)$, and $\sigma(\gamma, 3n)$, were measured for ^{55}Mn and ^{59}Co from threshold to 36.5 MeV, with a photon energy resolution which varied from 80 keV at the lowest to 170 keV at the highest energies measured. The source of radiation was the monoenergetic photon beam obtained from the annihilation in flight of fast positrons. The partial photoneutron cross sections were determined by neutron multiplicity counting, and the average neutron energies for $(\gamma, 1n)$ and $(\gamma, 2n)$ events were determined simultaneously with the cross-section data by the ring-ratio technique. The cross sections exhibit considerable but weak structure. Other nuclear information extracted from the data includes parameters of the giant dipole resonance, integrated cross sections and their moments, and nuclear symmetry energies. A comparison is made with previous experimental data for these nuclei as well as with theoretical predictions based upon hydrodynamic, vibrational, and dynamic collective models. None of these models fits the data for these odd-even nuclei satisfactorily; more theoretical work is needed for this nuclear mass region.

NUCLEAR REACTIONS ^{55}Mn , $^{59}\text{Co}(\gamma, n, 2n, 3n)$, $E_\gamma = 10 - 36.5$ MeV; measured 4π neutron yield, multiplicities, average energies for monoenergetic photons; $\sigma(E_\gamma, 1n)$, $\sigma(E_\gamma, 2n)$, $\sigma(E_\gamma, 3n)$, GDR parameters, integrated cross sections and moments, nuclear symmetry energies.

I. INTRODUCTION

The hydrodynamic model has had considerable success in explaining the general features of the giant dipole resonance (GDR) in medium-heavy and heavy nuclei, including its splitting into two resonances for statically deformed nuclei.¹ In particular, values for the intrinsic quadrupole moment Q_0 inferred from this splitting have been in good agreement with values obtained by Coulomb excitation and other methods. For lighter deformed nuclei, particularly those in the s - d shell, even moderate-resolution photonuclear measurements have revealed such a rich intermediate structure that attempts to apply the hydrodynamic model to obtain nuclear deformation parameters have been unsuccessful. For intermediate nuclei, such as those in the f - p shell however, previous low-resolution measurements appear to yield reasonable values for Q_0 . One of the goals of this high-resolution experiment ($\Delta E/E < 1\%$) was to test whether this simple analysis holds up under close scrutiny.

A corollary goal was to test the predictions of more sophisticated models, such as the vibrational model and the dynamic collective model (DCM). Indeed, it was the availability of theoretical predictions for the features of the GDR for ^{55}Mn and ^{59}Co (Ref. 2), together with the ready availability of pure monoisotopic samples, that determined the particular choice of these nuclei for the present

measurement.

A third goal was suggested by two unusual features of the photoneutron cross sections for the nearby isotopes of nickel, ^{58}Ni and ^{60}Ni , which were reported in an earlier paper from this Laboratory.³ These are (a) the small size of the photoneutron cross sections for ^{58}Ni (but not for ^{60}Ni), and (b) the appearance of unexpectedly sharp structure in the cross sections at relatively high excitation energies (as high as 25 MeV). To observe the latter, the high resolution of the present measurement was required, and we therefore looked for similar structure in ^{55}Mn and ^{59}Co .

There has been a good deal of experimental work on the photoneutron reactions for these nuclei reported previously, but these measurements (except for earlier results from this Laboratory⁴ for ^{59}Co) were performed with continuous bremsstrahlung radiation sources, with their inherent difficulties, and none of them was performed with energy resolution comparable to the present work. Also, only Ref. 4 employed neutron multiplicity counting to determine the $(\gamma, 1n)$ and $(\gamma, 2n)$ cross sections independently. Photoneutron cross-section measurements in the giant-resonance region since 1959 have been reported for ^{55}Mn by Parsons,⁵ Flournoy *et al.*,⁶ Ishkhanov *et al.*,⁷ and Carchon *et al.*,⁸ and for ^{59}Co by Flournoy *et al.*,⁹ Bazhanov *et al.*,¹⁰ Baciu *et al.*,¹¹ and Baciu *et al.*¹² A low-energy point for $\sigma(\gamma, n)$ for ^{59}Co has been reported by Hurst and Donahue.¹³

In addition, photoproton cross-section measurements have been reported for ^{55}Mn by Shoda *et al.*¹⁴ and for ^{59}Co by Cameron *et al.*¹⁵ [the latter obtained by detailed balance from $^{58}\text{Fe}(p, \gamma)$ data], and total photon-absorption cross sections have been reported for ^{55}Mn by Dolbilkin *et al.*¹⁶ and for ^{59}Co by Wyckoff *et al.*¹⁷ Finally, a measurement of the average neutron energy \bar{E}_n in the giant-resonance region for ^{55}Mn has been reported by Barrett *et al.*¹⁸ These earlier data will be discussed or compared with the present data below.

II. EXPERIMENT AND DATA REDUCTION

The experimental techniques and data-reduction procedures have been presented in detail elsewhere, the former in Refs. 1 and 3, the latter in Refs. 19 and 20; therefore, only those details pertinent to the present data will be given here.

The measurements were carried out with the monoenergetic photon beam obtained from the annihilation in flight of fast positrons from the Lawrence Livermore Laboratory Electron-Positron Linear Accelerator facility. The photoneutrons were detected with an efficient paraffin-and- BF_3 -tube 4π neutron detector. The partial photoneutron cross sections were determined by neutron multiplicity counting and the average neutron energies, and hence the neutron-detector efficiencies, were obtained for each multiplicity and for each data point by the ring-ratio technique. Two different positron converters were employed in the present experiment; one after the first accelerator section was used for taking the higher-energy (but poorer statistics) data, and one after the fourth section for the lower-energy (better statistics) data (see Ref. 3 for further details).

The nuclear samples were in the form of pure metal powder, contained in thin-walled cylindrical lucite containers 3.81 cm in diameter. The mass of the ^{55}Mn sample was 220 g and that of the ^{59}Co sample was 236 g (each was 4.0 moles). The samples were cycled alternatively into position along the photon beam line at the center of the 4π neutron detector by means of an eight-position sample changer, along with an empty lucite container and a standard sample for which the cross section is smooth, so that beam-tuning conditions were the same for all samples at each energy. In a high-resolution experiment like the one reported here, this technique is very valuable in that it eliminates extraneous peaks caused by short-term experimental drifts of any kind, and thus gives one confidence that any structure seen in the cross sections is real, and not an experimental artifact. The attenuation of the photon beam in the samples necessitated a correction to the data ranging from 30 to

TABLE I. Photoneutron threshold energies (in MeV). Values taken from Ref. 21.

Nucleus	$E_{\text{thr}}(\gamma, n)$	$E_{\text{thr}}(\gamma, pn)$	$E_{\text{thr}}(\gamma, 2n)$	$E_{\text{thr}}(\gamma, 3n)$
^{55}Mn	10.227	17.787	19.166	31.220
^{59}Co	10.454	17.408	19.027	30.404

40%, but introduced negligible uncertainty into the cross-section analysis.

The photon energy resolution varied from ~ 80 keV at 10 MeV to ~ 170 keV at 35 MeV, corresponding to the use of a 0.25-mm thick beryllium annihilation target and an incident positron beam analyzed to $\Delta p/p = 0.4\%$. The absolute energy scale was set with respect to the 17.3-MeV peak in the $^{16}\text{O}(\gamma, n)$ cross section and to many $(\gamma, 2n)$ thresholds. The threshold energies for the photoneutron reactions for ^{55}Mn and ^{59}Co are given in Table I (taken from Ref. 21), and are shown in the data plots by arrows. The threshold energies determined in the present measurements all agree, within the experimental limits, with these values.

Backgrounds from all sources, including those from empty Lucite containers, were measured and found to be small compared to the true counting rates (because of the massive samples and large cross sections) and thus introduced negligible uncertainties. Subtraction of the photoneutron yields resulting from positron bremsstrahlung was accomplished with the use of experimental runs taken with electron (instead of positron) beams. This

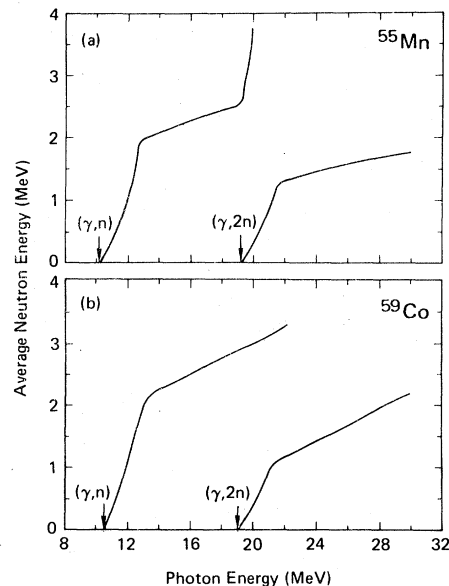


FIG. 1. Average single- and double-photoneutron energies plotted as functions of photon energy: (a) for ^{55}Mn ; (b) for ^{59}Co .

procedure introduced only small statistical uncertainties but did introduce a 2-to-4% systematic uncertainty in the electron-to-positron normalization factor.

The systematic uncertainty in the photon flux calibration was about 5% in the giant-resonance region and somewhat larger at 35 MeV. The uncertainty in the knowledge of the neutron detector efficiency usually was much less than 5%, but for single photoneutron events at energies above ~24 MeV and for double-photoneutron events above ~32 MeV, this latter uncertainty exceeds 10%. The resulting overall systematic uncertainty from all sources is no greater than 7% in the giant-resonance region but could reach 15% at the higher energies. The error bars in the cross-section plots represent statistical uncertainties only.

III. RESULTS AND DISCUSSION

A. Average photoneutron energies

The average neutron energies for $(\gamma, 1n)$ and $(\gamma, 2n)$ events derived from the ring-ratio data are shown, as functions of photon energy, in Fig. 1(a) for ^{55}Mn and in Fig. 1(b) for ^{59}Co . These data are in the form of solid lines, which represent the actual data in the energy regions where they are statistically best determined (see Ref. 19). One sees, as is typical for medium and heavy nuclei, a rapid rise from threshold followed by a much more gradual rise centered about a value characteristic of the excited compound nuclear system [the target nucleus for $(\gamma, 1n)$ events and the target-minus-one-neutron nucleus for $(\gamma, 2n)$ events]. These "characteristic" values are about 2.3 and 2.6 MeV for $(\gamma, 1n)$ events for ^{55}Mn and ^{59}Co , respectively, and about 1.6 and 1.7 MeV for $(\gamma, 2n)$ events, respectively. A rise in $\bar{E}_n(\gamma, 1n)$ above $E_{\text{thr}}(\gamma, 2n)$ is not unexpected, since the lower-energy neutrons are easily bled off into the $(\gamma, 2n)$ channel. Barrett *et al.*¹⁸ measured \bar{E}_n for ^{55}Mn for various bremsstrahlung end-point energies; their (bremsstrahlung-weighted integrated) results, e.g., about 2 MeV at a 20-MeV end-point energy, are in good agreement with the present data.

B. Cross sections

The photoneutron cross sections for ^{55}Mn are shown in Fig. 2 and for ^{59}Co in Fig. 3, as functions of photon energy. The total photoneutron cross sections $\sigma(\gamma, n_t) = \sigma[(\gamma, 1n) + (\gamma, 2n) + (\gamma, 3n)]$, shown in part (a) of the figures, have been fitted with two-component Lorentz curves, shown as solid lines in the figures, the parameters for which are given in Table II (more on this later). The single-photoneutron cross sections $\sigma(\gamma, 1n) = \sigma[(\gamma, n)$

$+$ $(\gamma, pn)]$, shown in part (b) of the figures, remain significantly greater than zero up to the highest energies measured, like the nickel isotopes (Ref. 3) and unlike nearly all nuclei of mass ≥ 90 (see Ref. 1). This shows either that there is a significant nonstatistical decay fraction of the compound system at energies just above the GDR or a substantial (γ, pn) cross section at these energies [note (Table I) that $E_{\text{thr}}(\gamma, pn) < E_{\text{thr}}(\gamma, 2n)$ for both of these

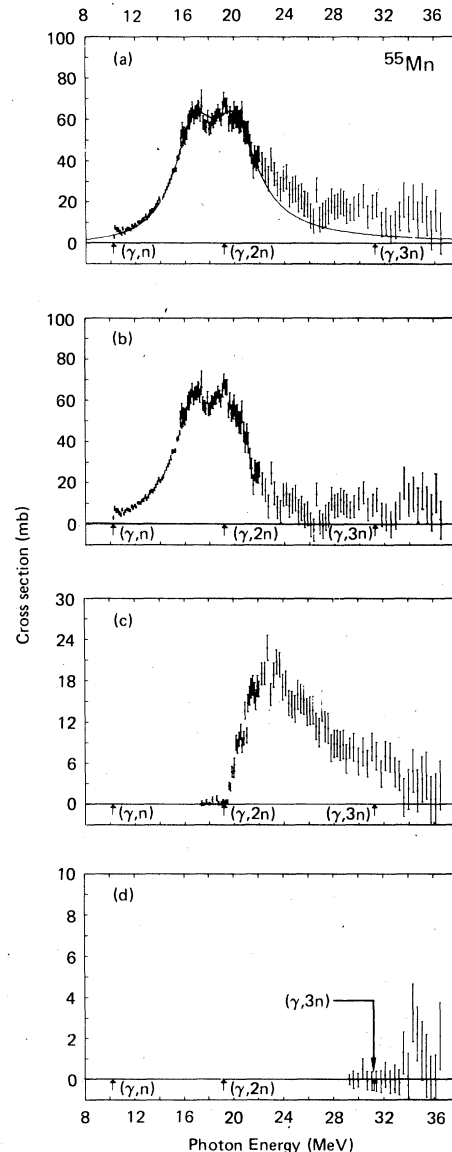


FIG. 2. Photoneutron cross sections for ^{55}Mn : (a) total photoneutron cross section $\sigma(\gamma, n_t) = \sigma[(\gamma, 1n) + (\gamma, 2n) + (\gamma, 3n)]$, together with a two-component Lorentz-curve fit to the data (solid line); (b) single-photoneutron cross section $\sigma(\gamma, 1n) = \sigma[(\gamma, n) + (\gamma, pn)]$; (c) double-photoneutron cross section $\sigma(\gamma, 2n)$; (d) triple-photoneutron cross section $\sigma(\gamma, 3n)$.

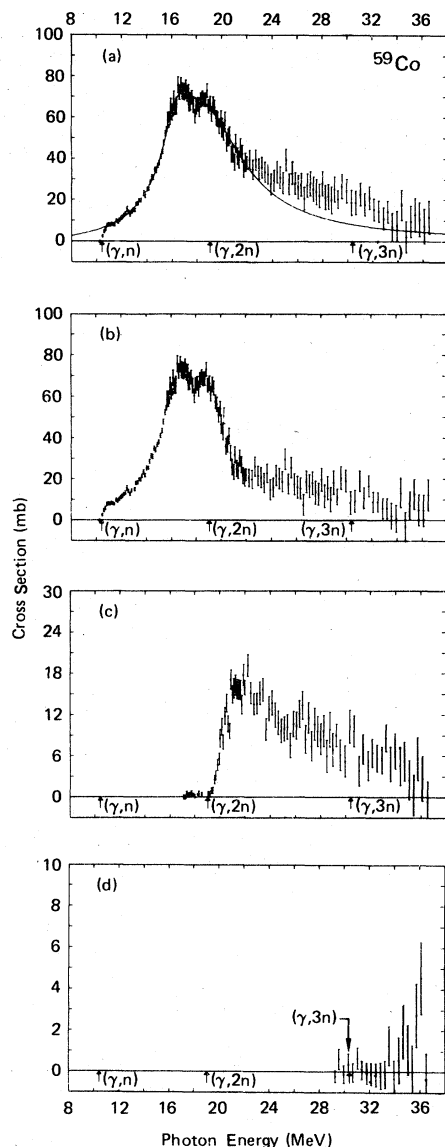


FIG. 3. Photoneutron cross sections for ^{59}Co : (a) $\sigma(\gamma, n_t)$, with a two-component Lorentz-curve fit; (b) $\sigma(\gamma, 1n)$; (c) $\sigma(\gamma, 2n)$; (d) $\sigma(\gamma, 3n)$.

nuclei], or both. We note here that there is appreciable “excess” cross section in $\sigma(\gamma, n_t)$ [part (a) of the figures] above the Lorentz-curve fits at energies greater than 21 MeV [the fitting interval

used was 14 to 21 MeV (see Ref. 1 for a discussion of the choice of fitting intervals)], and that both of these phenomena [the excess cross section and a large (γ, pn) fraction] can be explained by the presence of a broad giant quadrupole resonance at these energies (for further discussion of quadrupole effects in photoneutron cross sections, see Refs. 1, 19, 22, and especially Ref. 3). The $(\gamma, 2n)$ cross sections, shown in part (c) of the figures, also remain appreciable above the $(\gamma, 3n)$ thresholds, which is rarely the case for heavy nuclei. The $(\gamma, 3n)$ cross sections, shown in part (d) of the figures, are very small—in fact, scarcely significantly greater than zero—up to 36.5 MeV; this behavior also would be unusual for heavy nuclei.

Considerable weak structure appears in all the cross sections. Several weak peaks appear to be superposed on the leading edge of the GDR for both nuclei; the GDR itself is made up of two major peaks, but possibly with further fine structure superposed; and the cross section above the GDR appears to contain several broad structures, particularly for ^{55}Mn . For ^{55}Mn , there are low-energy peaks at 10.4, (11.0), 11.4, 13.3, 13.9, and 15.0 MeV; for ^{59}Co , at 11.0, 11.6, 12.4, (12.9), (13.8), (14.4), and (14.7) MeV (the parentheses indicate assignments that are questionable on statistical grounds). The main GDR peaks for ^{55}Mn are at 17.0 and 19.2 MeV, with possible smaller peaks at 18.7, 20.3, 21.1, and 22 MeV; for ^{59}Co , the main GDR peaks are at 17.1 and 18.7 MeV, with possible smaller peaks at 16.1 and 17.6 MeV. Above the GDR for ^{55}Mn , broad peaks appear to be located at about 24.5, 29.5, and 34.5 MeV; for ^{59}Co , no such suggestive structures appear, although there is plenty of “excess” cross section.

The average value of $\sigma(\gamma, n)$ near the peak of the GDR is about 65 mb for ^{55}Mn and about 70 mb for ^{59}Co . These values can be compared with the results of other measurements in the literature: Average GDR values obtained for ^{55}Mn are about 70 mb (Ref. 5), 75 mb (Ref. 6), 65 mb (Ref. 7), and 75 mb (Ref. 8); for ^{59}Co , about 90 mb (Ref. 6), 70 mb (Ref. 4), 80 mb (Ref. 9), 70 mb (Ref. 10), 75 mb (Ref. 11), and 95 mb (Ref. 12). We conclude that there is reasonable general agreement among the reported values of the cross section; the present results are slightly lower than average, and

TABLE II. Parameters of two-component Lorentz-curve fits to the GDR. The fitting interval used is 14 to 21 MeV.

Nucleus	$E_m(1)$ (MeV)	$\sigma_m(1)^a$ (mb)	$\Gamma(1)$ (MeV)	$E_m(2)$ (MeV)	$\sigma_m(2)^a$ (mb)	$\Gamma(2)$ (MeV)	χ^2
^{55}Mn	16.82 ± 0.10	51.4 ± 4.1	4.33 ± 0.63	20.09 ± 0.12	45.2 ± 2.6	4.09 ± 1.07	1.14
^{59}Co	16.43 ± 0.08	28.3 ± 5.4	2.73 ± 1.08	18.66 ± 0.25	58.4 ± 4.4	7.38 ± 0.79	1.11

^aUncertainties for σ_m given here are relative. The absolute uncertainties are 7%.

the results of Refs. 6 and 12 are on the high side. The value of 9.0 ± 0.8 mb at 10.83 MeV for $^{59}\text{Co}(\gamma, n)$ given in Ref. 13 is in agreement with the present result of 7.7 ± 0.9 mb. The only other measurement of $\sigma(\gamma, 2n)$ was that of Fultz *et al.*,⁴ who obtained a peak value for this cross section for ^{59}Co of ~ 20 mb, in agreement with the present results. Comparison of the structure found in the present measurements with that found in bremsstrahlung experiments (Refs. 7, 8, 11, and 12) will not be undertaken here; for the case of ^{55}Mn , see Ref. 8.

In order to evaluate the relative sizes of the (γ, n_i) and (γ, p) cross sections, one can refer to measurements of the total photon absorption cross section $\sigma(\gamma, \text{tot})$. For both ^{55}Mn (Ref. 16) and ^{59}Co (Ref. 17), these measurements yield $\sigma(\gamma, \text{tot}) \sim 90$ mb in the GDR region. These values together with the present photoneutron results yield $\sigma(\gamma, p)/(\gamma, n_i) \cong \frac{1}{3}$ or so, which agrees with the photoproton measurement of Ref. 14 and with the case for ^{60}Ni (see Ref. 3). Since other photoneutron measurements in this mass region^{4, 23-25} have yielded similar results, we conclude that ^{55}Mn and ^{59}Co are typical nuclei in this respect, and that ^{58}Ni (see Ref. 3) is unusual—in fact, unique among stable nuclei in this mass region. This conclusion enables us to treat the total photoneutron cross section $\sigma(\gamma, n_i)$ as representative of and equal to about $\frac{3}{4}$ of $\sigma(\gamma, \text{tot})$. [This is modified slightly by the 2-MeV-or-so upward displacement of $\sigma(\gamma, p)$ relative to $\sigma(\gamma, n)$ discussed below (Refs. 14 and 15).] Thus, in the discussion of integrated cross sections and giant-resonance parameters in the next four sections, we are able to treat those subjects without major uncertainties resulting from our imperfect knowledge of the photoproton cross sections, bearing in mind that the theories discussed in Sec. III D-F apply to $\sigma(\gamma, \text{tot})$, while the $\sigma(\gamma, n_i)$ data presented in this paper constitute most, but not all, of $\sigma(\gamma, \text{tot})$.

In general, photoproton cross sections, because of the Coulomb barrier, are not only small compared with photoneutron cross sections (for $A \geq 50$, say), but are displaced upward in energy by a few MeV, and the results of Refs. 14 and 15 bear out this assertion for both ^{55}Mn and ^{59}Co . This displacement has been related to the isospin splitting of the GDR as well, since the (larger) $T_<$ com-

ponent lies lower in energy and will decay by neutron emission, while the (smaller) $T_>$ component lies higher in energy and neutron decay of $T_>$ states can take place only through isospin mixing or to high-lying ($T_>$) states in the residual nucleus. The detailed discussion of isospin effects in Ref. 3 makes it clear, however, that the matter for these medium-mass nuclei is far from being a simple one, and therefore we refrain from further belaboring this topic here. In any case, the present data alone in the absence of detailed (γ, p) [not (γ, p_0)] cross sections, throw little light on the subject.

C. Integrated cross sections

The measured integrated cross sections for ^{55}Mn and ^{59}Co are given in Table III. Columns 3, 4, and 5 in this table list the integrated single-, double-, and triple-photoneutron cross sections, respectively; column 6 lists the ratio of the integrated double to total photoneutron cross sections; column 7 lists the measured integrated total photoneutron cross section in TRK sum-rule units, and column 8 lists the total area under the two-component Lorentz-curve fits to $\sigma(\gamma, n_i)$ in those units. The values listed in columns 7 and 8, when multiplied by about $\frac{4}{3}$ (see preceding section), give an indication of the amount of exchange-force enhancement of the dipole sum-rule values that might be needed to account for the GDR. The resulting values—about 1.2 TRK sum-rule units—are the same as the mean of many measurements on other nuclei made with monoenergetic photons.^{1, 26}

The integrated moments of the measured photoneutron cross sections σ_{-1} and σ_{-2} are given in columns 2 and 4, respectively, of Table IV. Because of the missing photoproton strength and its upward displacement in energy, the values for σ_{-1} should be multiplied by about 1.25 and those for σ_{-2} by about 1.15 before comparing them with values derived from $\sigma(\gamma, \text{tot})$ for other nuclei. The values of the quantities listed in columns 5 and 6 of Table IV, insofar as they are near to unity, can be thought of as figures of merit for the applicability of the Migdal sum rule,²⁷ which relates σ_{-2} to the nuclear polarizability and to the nuclear symmetry energy K . The last column gives values for the nuclear symmetry energy computed from this sum rule [which should be reduced somewhat

TABLE III. Integrated cross sections. $\sigma_{\text{int}}(\gamma, x) = \int \sigma(\gamma, x) dE_\gamma$, integrated from threshold to $E_{\gamma \text{max}}$.

Nucleus	$E_{\gamma \text{max}}$ (MeV)	$\sigma_{\text{int}}(\gamma, 1n)$ (MeV-mb)	$\sigma_{\text{int}}(\gamma, 2n)$ (MeV-mb)	$\sigma_{\text{int}}(\gamma, 3n)$ (MeV-mb)	$\frac{\sigma_{\text{int}}(\gamma, 2n)}{\sigma_{\text{int}}(\gamma, n_i)}$	$\frac{\sigma_{\text{int}}(\gamma, n_i)}{60NZ/A}$	$\frac{\frac{1}{2}\pi[\sigma_m(1)\Gamma(1) + \sigma_m(2)\Gamma(2)]}{60NZ/A}$
^{55}Mn	36.5	567	163	3	0.222	0.90	0.78
^{59}Co	36.5	653	150	4	0.186	0.92	0.91

TABLE IV. Integrated cross-section moments. $\sigma_{-1} = \int \sigma(\gamma, n_t) E_\gamma^{-1} dE_\gamma$ and $\sigma_{-2} = \int \sigma(\gamma, n_t) E_\gamma^{-2} dE_\gamma$, integrated from threshold to $E_{\gamma \text{ max}}$.

Nucleus	σ_{-1} (mb)	$\sigma_{-1} A^{-4/3}$ (mb)	σ_{-2} (mb-MeV $^{-1}$)	$\frac{\sigma_{-2}}{0.00225A^{5/3}}$	$\frac{\sigma_{-2}K}{0.05175A^{5/3}}$	$\frac{0.05175A^{5/3}}{\sigma_{-2}}$
						(MeV)
^{55}Mn	36.4	0.174	1.93	1.08	0.91 ^a	21.3
^{59}Co	40.1	0.174	2.14	1.06	0.90 ^a	21.7

^aThe values used for the nuclear symmetry energy K are from Table VI.

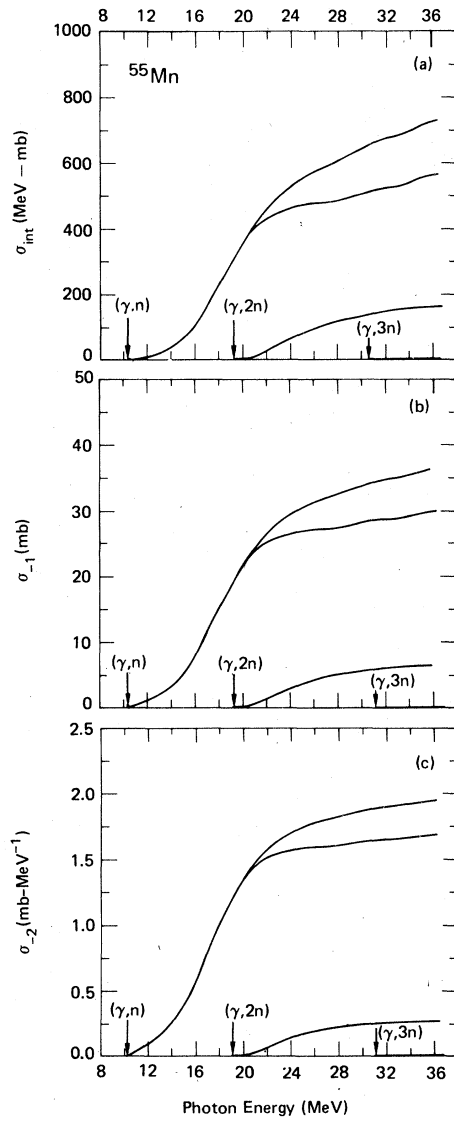


FIG. 4. Running sums of integrated photoneutron cross sections and their moments for ^{55}Mn : (a) $\sigma_{\text{int}} = \int \sigma dE$ for $\sigma(\gamma, n_t)$ (top), $\sigma(\gamma, 1n)$ (next to top), $\sigma(\gamma, 2n)$ (next to bottom), and $\sigma(\gamma, 3n)$ (bottom); (b) $\sigma_{-1} = \int \sigma E_\gamma^{-1} dE_\gamma$; (c) $\sigma_{-2} = \int \sigma E_\gamma^{-2} dE_\gamma$.

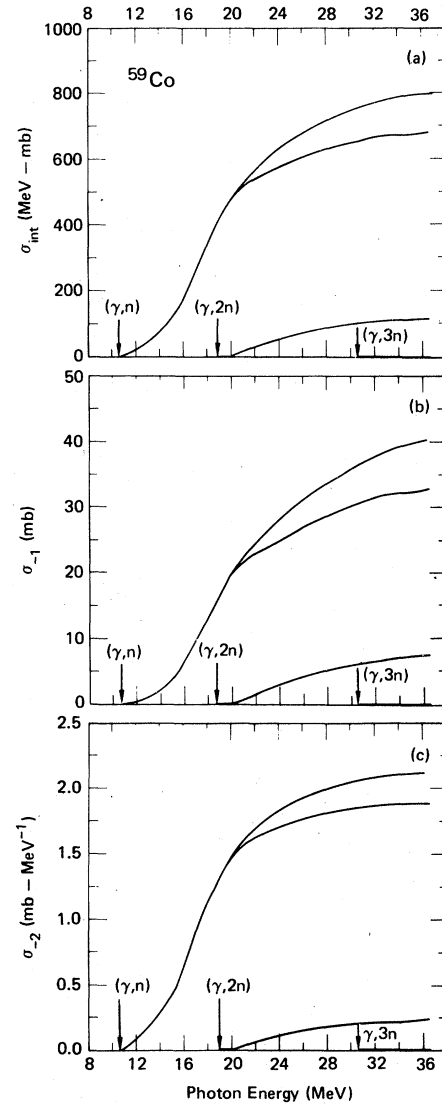


FIG. 5. Running sums of integrated cross sections for ^{59}Co : (a) σ_{int} ; (b) σ_{-1} ; (c) σ_{-2} .

by taking into account the contribution of $\sigma(\gamma, p)$ to σ_{-2}].

The present experimental data on all the integrated cross sections and their moments are shown in Fig. 4 for ^{55}Mn and in Fig. 5 for ^{59}Co , in the form of running sums of the quantities plotted as functions of the photon energy up to which they are integrated. This form of displaying the integrated cross-section data is useful for information-retrieval purposes, and also shows whether and how well the various plotted quantities approach asymptotic behavior at high photon energies. These figures show that in spite of the existence of nonzero cross sections at the highest photon energies employed in this experiment, the integrated photoneutron cross sections (and of course, their moments) indeed appear to be approaching asymptotic values at energies not too far in excess of 40 MeV or so. This is important, of course, for the above discussion of sum rules.

D. Giant-resonance parameters—the hydrodynamic model

The classic collective description of the GDR predicts that $\sigma(\gamma, \text{tot})$ for deformed nuclei is characterized as the sum of two Lorentz-shaped curves,^{1, 28}

$$\sigma(\gamma, \text{tot}) = \sum_{i=1}^2 \left(\sigma_m(i) / 1 + \frac{[E_\gamma^2 - E_m^2(i)]^2}{E_\gamma^2 \Gamma^2(i)} \right),$$

where $\sigma_m(i)$, $E_m(i)$, and $\Gamma(i)$ are the peak height, resonance energy, and full width of the i th Lorentz curve. Although this classic approach, which works very well for statically deformed (rare-earth and actinide) nuclei,^{1, 29, 30} has been applied in the past to nuclei in the mass region near ^{55}Mn and ^{59}Co ,^{1, 4-6, 9, 10, 23, 31} it is by no means clear that this procedure would stand the test of close experimental scrutiny imposed by a high-resolution measurement. In particular, since ^{55}Mn and ^{59}Co are described better as vibrational than as rotational nuclei, one expects^{19, 32} a two-component Lorentz-curve fit to be at best an approximation to the actual case. In order to test this idea, the present $\sigma(\gamma, n_t)$ data were fitted with two-component Lorentz curves; the resulting parameters are given in Table II. Although the χ^2 values for these fits are good, one can see from the values for the σ_m 's and Γ 's that the area ratios $R_A = \sigma_m(1)\Gamma(1) / \sigma_m(2)\Gamma(2)$ for these nuclei are far from the value of 0.5 predicted by the hydrodynamic model. [Note that if the (γ, p) contribution to $\sigma(\gamma, \text{tot})$ were taken into account the values for R_A would be somewhat smaller. However, the fact that one value for R_A is much larger than 0.5 and the other is much smaller means that the relatively small corrections which would result from the inclusion of

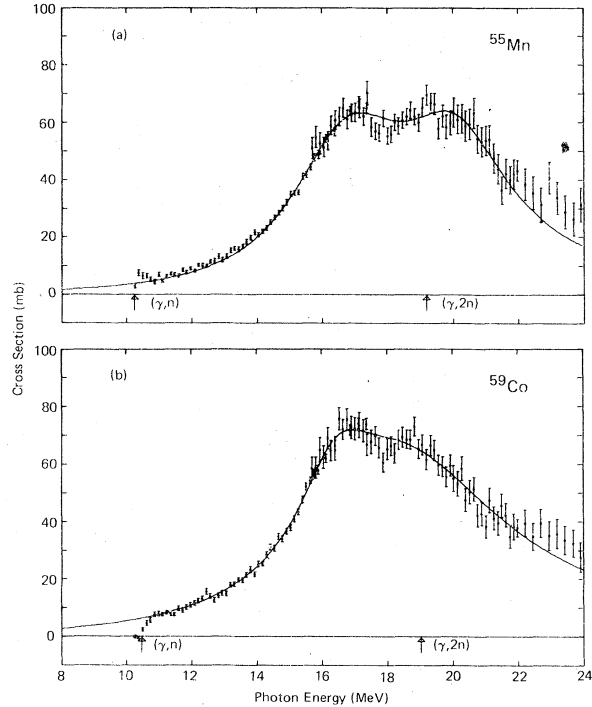


FIG. 6. Total photoneutron cross sections, with two-component Lorentz-curve fits: (a) for ^{55}Mn ; (b) for ^{59}Co . Although the theoretical model is strictly valid only for $\sigma(\gamma, \text{tot})$, the curve shown here was scaled to fit the measured $\sigma(\gamma, n_t)$ data (see Sec. III B in the text and Table III).

$\sigma(\gamma, p)$ are not important.] Furthermore, it can be seen from Fig. 6, in which the portions of $\sigma(\gamma, n_t)$ only up to 24 MeV are plotted [for ^{55}Mn in part (a) and for ^{59}Co in part (b)] together with these two-component Lorentz curves, that there is a poor match between the curves and the data in the critically important peak region of the GDR. In particular, such fits cannot reproduce the sharp minima that appear in the cross-section data at 18.0 MeV for ^{55}Mn and at 17.9 MeV for ^{59}Co . Thus, despite the overall goodness of fit implied by the low χ^2 values, one cannot take these two-component Lorentz-curve fits very seriously.

This being the case—that one cannot character-

TABLE V. Parameters of one-component Lorentz-curve fits to the GDR. The fitting interval used is 14 to 21 MeV.

Nucleus	E_m (MeV)	σ_m^a (mb)	Γ (MeV)	χ^2
^{55}Mn	18.04 ± 0.09	68.5 ± 1.3	6.59 ± 0.27	5.21
^{59}Co	17.68 ± 0.56	76.6 ± 1.2	6.07 ± 0.18	3.66

^aUncertainties for σ_m given here are relative. The absolute uncertainties are 7%.

TABLE VI. Parameters for classical theories. All quantities given in MeV.

Nucleus	α^a	β^b	K^c
^{55}Mn	68.6	35.2	19.5
^{59}Co	68.8	34.9	19.5

^aHydrodynamic parameter, defined by $E_m = \alpha A^{-1/3}$.

^bCollective parameter, defined by $E_m = \beta A^{-1/6}$.

^cNuclear symmetry energy, computed from

$$K = 9.935 \times 10^{-4} \frac{A^{3/3}}{NZ} \frac{E_m^2}{1 - (\Gamma/2E_m)^2}.$$

ize the GDR well with two-component Lorentz curves—we have chosen, for purposes of determining an overall GDR energy, simply to use the results of one-component Lorentz-curve fits to $\sigma(\gamma, n_t)$ in the GDR region; these parameters are given in Table V. It is noted here that the values for E_m from these fits, namely, 18.0 and 17.7 MeV for ^{55}Mn and ^{59}Co , respectively, are somewhat lower than the harmonic mean energies $E_H = \sigma_{\text{int}} / \sigma_{-1}$, which are 20.1 MeV for both nuclei, or the average energies $E_A = \sigma_{-1} / \sigma_{-2}$, which are 18.9 MeV for ^{55}Mn and 18.7 MeV for ^{59}Co . Had we taken the contribution of $\sigma(\gamma, p)$ into account, the various values for the GDR energy would move up a bit and bunch together more closely. Table VI lists values for the GDR parameters for classical theories based on the Lorentz parameters of Table V. If one in particular compares the values for the nuclear symmetry energy K given in the last column of Table VI with those given in the last column of Table IV, one notes roughly a 10% discrepancy. However, the preceding discussion makes it clear that the former values are too low and the latter too high, so that this discrepancy tends to disappear (indeed, one even can generate a discrepancy in the other direction); thus, it is quite reasonable to conclude that the results of these two methods for obtaining the nuclear symmetry energy converge to yield values near 20 MeV for both of these nuclei.

E. The vibrational model of Kerman and Quang

Some time ago, Kerman and Quang³³ outlined a method for relating the parameters of the giant

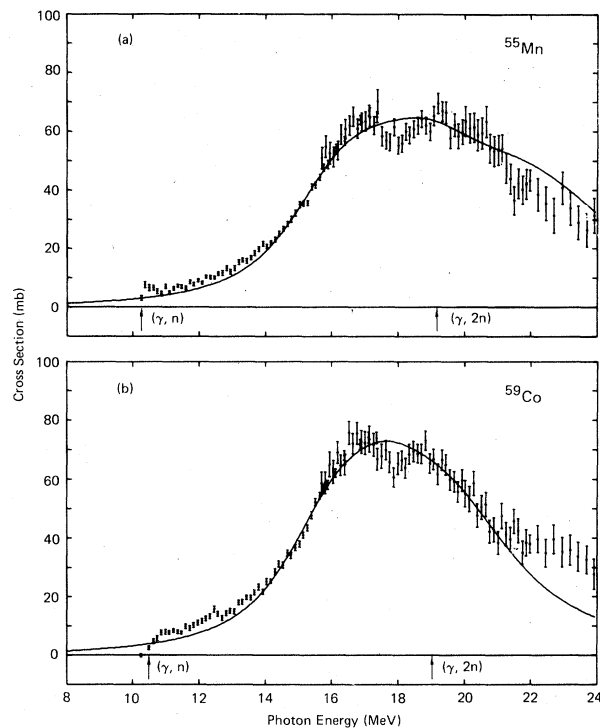


FIG. 7. Total photoneutron cross sections, with Kerman-Quang fits: (a) for ^{55}Mn ; (b) for ^{59}Co . Although the theoretical model is strictly valid only for $\sigma(\gamma, \text{tot})$, the curve shown here was scaled to fit the measured $\sigma(\gamma, n_t)$ data (see Sec. III B in the text and Table VII).

dipole resonance of a nucleus to its ground-state vibrational character. Specifically, they depicted the shape of the giant resonance for a spherical vibrational nucleus (one whose ground-state equilibrium deformation is zero, but whose rms deformation is nonzero) as a superposition of Lorentz curves, each having an intrinsic width which corresponds to the case which would obtain if the nucleus were infinitely stiff. The position of these Lorentzians is modulated, however, by a probability function (taken to be a Gaussian), centered at the energy corresponding to the equilibrium shape, thus resulting in a broadening of the giant resonance.

For a spherical vibrational nucleus, this reduces the number of parameters necessary to fit

TABLE VII. Kerman-Quang parameters. The fitting interval used is 14 to 21 MeV.

Nucleus	E_m (MeV)	Γ_{intr} (MeV)	β_0	F^a	χ^2
^{55}Mn	18.89 ± 0.38	3.23 ± 0.17	0.55 ± 0.07	0.87 ± 0.10	2.07
^{59}Co	17.74 ± 0.05	3.34 ± 0.21	0.37 ± 0.02	0.70 ± 0.01	1.81

^a F is expressed in TRK sum-rule units ($60NZ/A$ MeV-mb). The uncertainties given are relative; the absolute uncertainties are 7%.

the giant resonance from six (E_m , Γ , and σ_m for two Lorentz curves), as in the hydrodynamic theory for rotational nuclei, to four: E_m , the intrinsic width Γ_{int} , the ground-state vibrational parameter β_0 (as obtained from Coulomb-excitation measurements, for example), and F , an overall normalization factor proportional to the dipole sum rule. These parameters have been determined for ^{55}Mn and ^{59}Co by fitting the present $\sigma(\gamma, n_t)$ data, as was done earlier³⁴ for the preliminary data available then. These fits are shown in Fig. 7 [part (a) for ^{55}Mn and part (b) for ^{59}Co], and correspond to the parameters given in Table VII.

We see, from Table VII, that the χ^2 values for these four-parameter fits are better than the three-parameter fits of Table V but not as good as the six-parameter fits of Table II. In this sense, the Kerman-Quang approach can be said to be moderately successful. However, the values for β_0 of Table VII are unrealistically large, and a glance at Fig. 7 shows that even with these large values for β_0 , this approach fails [as before (Ref. 34)] to reproduce the sharp minima in the (γ, n_t) cross sections.

F. The dynamic collective model

The dynamic collective treatment of the giant resonance³⁵ results in the sharing of the dipole strength among several states which arise from terms in the nuclear Hamiltonian which specifically describe the coupling between the dipole vibrations on the one hand and the vibrational and rotational degrees of freedom of the nucleus on the other. These states appear as "satellites" to the main giant-resonance state(s) for stiff spherical and statically deformed nuclei, although they are more distinctive for the softer vibrational nuclei. Like the elementary hydrodynamic theory, however, this model says nothing about the widths (which characterize the damping of the giant-resonance states into the nuclear continuum) of the various peaks. Consequently, the question of inter-

TABLE VIII. DCM input parameters from Ref. 2, corresponding to quadrupole energy $E_2=1.3$ MeV and deformation parameter $\beta_0=0.22$, for ^{55}Mn and ^{59}Co .

E_k^a (MeV)	E_k^b (MeV)	ϕ_k^2 (relative units)
16.60	16.70	0.52
18.47	18.57	0.24
19.45	19.55	0.03
20.06	20.16	0.14
21.54	21.64	0.06

^aValues for ^{55}Mn , corresponding to dipole energy $E_1=18.2$ MeV.

^bValues for ^{59}Co , corresponding to $E_1=18.3$ MeV.

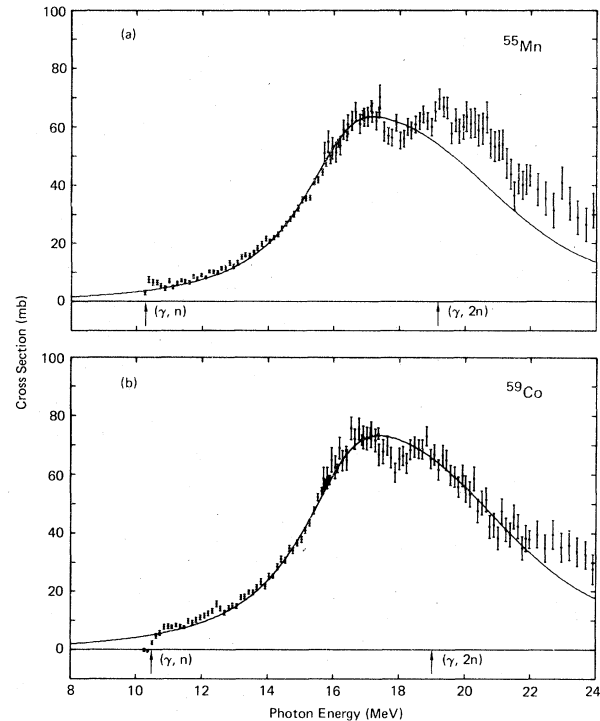


FIG. 8. Total photoneutron cross sections, with DCM fits: (a) for ^{55}Mn ; (b) for ^{59}Co . Although the theoretical model is strictly valid only for $\sigma(\gamma, \text{tot})$, the curve shown here was scaled to fit the measured $\sigma(\gamma, n_t)$ data (see Sec. III B in the text and Table IX).

mediate structure in the giant resonance of medium and heavy vibrationally or statically deformed nuclei is ambiguous theoretically, and has been the subject of many experimental studies.

Huber *et al.*² have calculated the distribution of strength in the GDR for ^{55}Mn and ^{59}Co within the framework of the DCM; their predictions for the energies and relative strengths for the dipole states which should constitute the GDR for these nuclei are given in Table VIII. In order to best fit these predictions to the data, the width of the lines was allowed to vary, along with the absolute normalization of the summed strength. (The data were fitted with a constant width for every line for each nucleus.) The resulting fitted curves are shown, together with the $\sigma(\gamma, n_t)$ data, in Fig. 8 [part (a)

TABLE IX. Parameters of DCM fits to the GDR. The fitting interval used is 14 to 21 MeV.

Nucleus	Width (MeV)	Normalization constant	χ^2
^{55}Mn	4.10	0.886	4.53
^{59}Co	4.41	0.858	1.37

for ^{55}Mn and part (b) for ^{59}Co], and the parameters resulting from these two-parameter fits are given in Table IX. The χ^2 values, given in the last column of the table, show that the fit to the ^{59}Co data is quite good, but the fit to the ^{55}Mn data is much worse.

Since the time that Ref. 2 was published, considerable progress has been made in the DCM treatment via its relation to the potential-energy-surface concept.^{36,37} One constructs such a surface for a nucleus by fitting its low-energy spectrum and then uses this surface to deduce the collective Hamiltonian for that nucleus, from which one can compute, using the DCM, the energies and strengths for the dipole absorption lines for the nucleus. Greiner *et al.*³⁸ have performed such calculations for the even-even nuclei in the Mn-Co region, from which one could interpolate to find the GDR strength distributions for ^{55}Mn and ^{59}Co . It turns out that by interpolating between ^{54}Co and ^{56}Fe one produces a strength distribution for ^{55}Mn not very much different from that of Ref. 2 (except for an energy shift, which can be taken into account). But for ^{59}Co , one is faced with a more formidable problem: The potential-energy surfaces (and hence the dipole strength distributions)

for ^{58}Fe and ^{60}Ni are strikingly different, the former having a deep prolate minimum and the latter being a spherical vibrator. This indicates that a phase transition takes place as one removes a pair of protons from the closed subshell nucleus ^{60}Ni , and one does not know on which side of this phase transition to place ^{59}Co (or whether it lies midway between). This theoretical ambiguity can be resolved only by a detailed potential-energy-surface calculation for ^{59}Co itself, which is a difficult undertaking. It would be interesting to see the results of such a calculation, and thus to test, with the present data, whether and where such a phase transition takes place.

Preliminary accounts of this work have appeared in Refs. 26, 34, 39, and 40. The present data supercede those presented in all of these earlier accounts. We thank Mr. D. L. Olsen for help with part of the data analysis, and Professor Walter Greiner for valuable discussions and suggestions. We also wish to thank the late Dr. S. C. Fultz for suggesting and participating in the planning for these measurements. Work performed under the auspices of the U. S. Department of Energy under Contract No. W-7405-ENG-48.

- ¹B. L. Berman and S. C. Fultz, *Rev. Mod. Phys.* **47**, 713 (1975).
- ²M. G. Huber, M. Danos, H. J. Weber, and W. Greiner, *Phys. Rev.* **155**, 1073 (1967).
- ³S. C. Fultz, R. A. Alvarez, B. L. Berman, and P. Meyer, *Phys. Rev. C* **10**, 608 (1974).
- ⁴S. C. Fultz, R. L. Bramblett, J. T. Caldwell, N. E. Hansen, and C. P. Jupiter, *Phys. Rev.* **128**, 2345 (1962).
- ⁵R. W. Parsons, *Can. J. Phys.* **37**, 1344 (1959).
- ⁶P. A. Flournoy, R. S. Tickle, and W. D. Whitehead, *Phys. Rev.* **120**, 1424 (1960).
- ⁷B. S. Ishkhanov, I. M. Kapitonov, E. V. Lazutin, I. M. Piskarev, and O. P. Shevchenko, *Izv. Akad. Nauk Fiz.* **34**, 2228 (1970) [*Bull. Acad. Sci. USSR—Phys.* **34**, 1988 (1970)].
- ⁸R. Carchon, J. Devos, R. Van De Vyver, C. Van Deynse, and H. Ferdinande, *Nucl. Phys.* **A223**, 416 (1974).
- ⁹E. B. Bazhanov, A. P. Komar, and A. V. Kulikov, *Zh. Eksp. Teor. Fiz.* **46**, 1497 (1964) [*Sov. Phys. JETP* **19**, 1014 (1964)].
- ¹⁰G. Baciú, G. C. Bonazzola, B. Minetti, C. Molino, L. Pasqualini, and G. Piragino, *Nucl. Phys.* **67**, 178 (1965).
- ¹¹B. I. Goryachev, B. S. Ishkhanov, I. M. Kapitonov, I. M. Piskarev, V. G. Shevchenko, and O. P. Shevchenko, *Izv. Akad. Nauk Fiz.* **33**, 1736 (1969) [*Bull. Acad. Sci. USSR—Phys.* **33**, 1588 (1969)].
- ¹²G. Baciú, D. Catană, C. Deberth, C. Iiescu, and B. Cîrstoiu, *Nucl. Phys.* **A167**, 177 (1971).
- ¹³R. R. Hurst and D. J. Donahue, *Nucl. Phys.* **A91**, 365 (1967).
- ¹⁴K. Shoda, K. Abe, T. Ishizuka, N. Kawamura, M. Oyamada, and B. N. Sung, *J. Phys. Soc. Jpn.* **25**, 664 (1968).
- ¹⁵C. P. Cameron, N. R. Roberson, D. G. Rickel, R. D. Ledford, H. R. Weller, R. A. Blue, and D. R. Tilley, *Phys. Rev. C* **14**, 553 (1976).
- ¹⁶B. S. Dolbilkin, A. I. Isakov, V. I. Korin, and L. E. Lazareva, *Zh. Eksp. Teor. Fiz. Pis'ma Red.* **10**, 365 (1969) [*JETP Lett.* **10**, 231 (1969)].
- ¹⁷J. M. Wyckoff, B. Ziegler, H. W. Koch, and R. Uhlig, *Phys. Rev.* **137**, B576 (1965).
- ¹⁸R. F. Barrett, J. R. Birkelund, B. J. Thomas, K. S. Lam, and H. H. Thies, *Nucl. Phys.* **A210**, 355 (1973).
- ¹⁹B. L. Berman, D. D. Faul, R. A. Alvarez, P. Meyer, and D. L. Olson, *Phys. Rev. C* **19**, 1205 (1969).
- ²⁰J. G. Woodworth, K. G. McNeill, J. W. Jury, R. A. Alvarez, B. L. Berman, D. D. Faul, and P. Meyer, Lawrence Livermore Laboratory Report No. UCRL-77471, 1978 (unpublished).
- ²¹A. H. Wapstra and K. Bos, *At. Data Nucl. Data Tables* **19**, 175 (1977).
- ²²S. C. Fultz, B. L. Berman, J. T. Caldwell, R. L. Bramblett, and M. A. Kelly, *Phys. Rev.* **186**, 1255 (1969).
- ²³S. C. Fultz, R. L. Bramblett, J. T. Caldwell, and R. R. Harvey, *Phys. Rev.* **133**, B1149 (1964).
- ²⁴R. E. Sund, M. P. Baker, L. A. Kull, and R. B. Walton, *Phys. Rev.* **176**, 1366 (1968).

- ²⁵P. Carlos, H. Beil, R. Bergère, J. Fagot, A. Leprêtre, A. Veysièrre, and G. V. Solodukhov, Nucl. Phys. A258, 365 (1976).
- ²⁶B. L. Berman, Lawrence Livermore Laboratory Report No. UCRL-78482, 1976 (unpublished).
- ²⁷J. S. Levinger, *Nuclear Photo-Disintegration* (Oxford Univ. Press, London, 1960), p. 51.
- ²⁸M. Danos, Nucl. Phys. 5, 23 (1958).
- ²⁹B. L. Berman, M. A. Kelly, R. L. Bramblett, J. T. Caldwell, H. S. Davis, and S. C. Fultz, Phys. Rev. 185, 1576 (1969).
- ³⁰J. T. Caldwell, E. J. Dowdy, B. L. Berman, R. A. Alvarez, and P. Meyer (unpublished).
- ³¹B. M. Spicer, Aust. J. Phys. 11, 490 (1958).
- ³²B. L. Berman, R. L. Bramblett, J. T. Caldwell, H. S. Davis, M. A. Kelly, and S. C. Fultz, Phys. Rev. 177, 1745 (1969).
- ³³A. K. Kerman and H. K. Quang, Phys. Rev. 135, B883 (1964).
- ³⁴D. D. Faul and B. L. Berman, Bull. Am. Phys. Soc. 19, 110 (1974).
- ³⁵M. Danos and W. Greiner, Phys. Rev. 134, B284 (1964).
- ³⁶V. Rezwani, M. Brand, R. Sedlmayr, L. V. Bernus, U. Schneider, and W. Greiner, in *Proceedings of the International Conference on Nuclear Structure Studies using Electron Scattering and Photoreaction*, edited by K. Shoda and H. Ui (Tohoku University, Sendai, Japan, 1972), p. 235.
- ³⁷R. Sedlmayr, M. Brand, V. Rezwani, and W. Greiner, in *Proceedings of the International Conference on Photonuclear Reactions and Applications*, edited by B. L. Berman (Lawrence Livermore Laboratory, Livermore, 1973), p. 1049.
- ³⁸W. Greiner, private communication.
- ³⁹R. A. Alvarez, B. L. Berman, F. H. Lewis, Jr., and P. Meyer, Bull. Am. Phys. Soc. 19, 110 (1974).
- ⁴⁰R. A. Alvarez, B. L. Berman, F. H. Lewis, and P. Meyer, in *Proceedings of the International Conference on Photonuclear Reactions and Applications*, edited by B. L. Berman (Lawrence Livermore Laboratory, Livermore, 1973), pp. 545 and 547.